Taylor, Stewart J. and Haw, Mark D. and Sefcik, Jan and Fletcher, Ashleigh J. (2015) Effects of secondary metal carbonate addition on the porous character of resorcinol-formaldehyde xerogels. Langmuir, 31 (50). pp. 13571-13580. ISSN 0743-7463 , http://dx.doi.org/10.1021/acs.langmuir.5b02483

Effects of secondary metal carbonate addition on the porous character of resorcinol-formaldehyde xerogels

*Stewart J. Taylor, Mark D. Haw, Jan Sefcik and Ashleigh J. Fletcher**

Department of Chemical and Process Engineering, University of Strathclyde, Glasgow, G1 1XJ

ABSTRACT:

A deeper understanding of the chemistry and physics of growth, aggregation and gelation processes involved in the formation of xerogels is key to providing greater control of the porous characteristics of such materials, increasing the range of applications for which they may be utilised. Time-resolved dynamic light scattering has been used to study the formation of resorcinol-formaldehyde gels in the presence of combinations of Group I (Na and Cs) and Group II (Ca and Ba) metal carbonates. It was found that the combined catalyst composition, including species and times of addition, is crucial in determining the end properties of the xerogels, via its effect on growth of clusters involved in formation of the gel network. Combination materials have textural characteristics within the full gamut offered by each catalyst alone; however, in addition, combination materials which retain the small pores associated with sodium carbonate catalysed xerogels exhibit a narrowing of the pore size distribution, providing an increased pore volume within an application-specific range of pore sizes. We also show evidence of pore size tunability while maintaining ionic strength, which significantly increases the potential of such systems for biological applications.

Introduction

Porous materials are often used in applications such as catalyst supports,[1] gas storage,[2] separations[3] and fuel cells.[4] The internal structure of these materials needs to be finely controlled, to give the pore sizes and connectivity required for the particular application. Porous materials can be made through a sol-gel route, where chemical reactions, such as polymerization, and physical processes, such as aggregation, occur simultaneously, resulting in the formation of a porous, solid network. The complexity of these competing chemical and physical processes means that the current understanding of the gel structure formation is limited and, therefore, fine tuning the textural properties of these porous materials remains a challenge. One promising type of sol-gel based porous material is based on resorcinol-formaldehyde (RF) gels. This paper provides novel insight into the formation of these gels, with the aim of providing improved understanding and tailoring of the porous characteristics towards particular applications.

The sol-gel polycondensation of resorcinol and formaldehyde, in the presence of sodium carbonate (Na_2CO_3) acting as a base was first published in 1989,[5] showing the production of a solid 3D network with water entrained within the porous system. Exchange of the water for acetone, followed by drying with supercritical carbon dioxide, resulted in a dried gel with very low density, large surface area and high pore volume. Subsequent pyrolysis in an inert atmosphere rendered the material electrically conductive, through the measured removal of non-carbon species. This transformation allowed for the use of these carbon materials in applications such as fuel cells,[6] where a conductive material with controlled porosity is required.

The mechanism subsequently proposed for the sol-gel synthesis involved two main stages.[7] Firstly, the base promotes the reaction between resorcinol and formaldehyde to produce

47 mono-, di-, and tri-substituted resorcinol known as hydroxymethyl derivatives; these
48 intermediates then undergo polycondensation into growing oligomers, which form clusters
49 that, through cross-linking, make up the gel structure. Detailed examination of this
50 mechanism has resulted in the development of a cluster growth model, wherein the size of the
51 clusters is thermodynamically controlled, while the kinetics of the reaction determines the
52 number concentration of clusters that form.[8] The sol-gel process is highly adaptable, allowing
53 a number of process variables to be altered; including the molar ratio of resorcinol to
54 formaldehyde, the total solids content, also known as dilution, or the type and quantity of
55 base used.[9, 10]

56 While the base of choice in the formation of RF gels is typically Na_2CO_3,[9] many other
57 reaction promoting media, both acidic and basic, have been utilized. While acids are less
58 common than bases, both mineral, e.g. nitric acid,[11] and organic acids, such as acetic acid,[12]
59 have seen use. More common are alternative bases, making use of lithium and potassium
60 cations or hydroxide anions in place of the typical sodium and carbonate.[13, 14] Carbonates of
61 the Group II metals have also been used to prepare RF gels, however, their use has been
62 limited in comparison to the Group I metals.[15, 16] Use of a Group II metal carbonate results in
63 larger pore sizes than an equivalent base concentration of Group I carbonate, a phenomenon
64 attributed to electrostatic effects as a result of the differing cation charges.[13] However, a
65 much more limited understanding of the gelation process in the presence of a Group II
66 carbonate is available.

67 The addition of an acid or base, and the accompanying pH change has been widely
68 recognized as highly influential in the gel formation process,[9, 10] and as such, only a limited
69 range of pH values will produce a viable gel structure. For bases, this lies between pH 5.5 and
70 7.5,[10, 17] while for acids the range falls between pH 1 and 4.[18, 19] Out with these regions, the
71 gel formed will be non-porous (> 7.5)[20] or take too long to form (4 – 5.5).[18] Alternatively, too

72 acidic an initial value, i.e. pH < 1, will cause the precipitation of reactants before a gel can
73 form.[10] Initial pH is, therefore, controlled by altering the amount of acid or base added, with
74 this value typically expressed as a molar ratio of resorcinol to 'catalyst' (R/C), with lower
75 ratios corresponding to higher catalyst concentrations. For Na_2CO_3, R/C values will typically
76 fall between 50 and 3000, with concentration influencing the porous properties of the final
77 gel.[9, 10] An increase in R/C leads to an increase in pore size, as a result of a reduction in the
78 number of clusters formed, and which can subsequently grow to larger sizes.

79 Lambert *et al*. and Laskowski *et al*. investigated double catalyzed RF gel formation.[21, 22].
80 Initially, the gel was catalyzed using a base, before an acid was added part way through the
81 gelation process, causing a significant reduction in gel time due to additional promotion of
82 the polymerization and cross-linking processes. However, both studies found that this
83 synthesis produced very broad pore size distributions, stretching from approximately 10 nm
84 to 100 nm.

85 Feng *et al*. studied the dual catalyst process further, by also investigating a base-base route
86 and comparing this to a standard single catalyzed gel.[23] In agreement with the works of
87 Lambert *et al*.[21] and Laskowski *et al*.,[22] the addition of an acid produced a broadening of the
88 pore size distribution. Interestingly, the addition of second quantity of base also caused a
89 broadening of the distribution, whilst simultaneously shifting the distribution to a larger
90 average pore size.

91 Dynamic Light Scattering (DLS) has been used to study the formation RF gels.[8, 24] In
92 agreement with Gaca *et al*.,[25] we previously found that cluster growth rate was
93 thermodynamically driven, being independent of catalyst concentration for lithium, sodium
94 and potassium carbonate, while the catalyst concentration determines the number density of
95 clusters through kinetic means.[25] Hence, high R/C values produce a lower number

concentration of clusters, which grow to larger sizes before reaching the volume fraction necessary to form a gel.

The aim of this work was to study the formation of RF gels when catalyzed using a Group II metal carbonate, allowing comparison with previously obtained results using Group I metal carbonate catalysts. Furthermore, the effect of secondary addition of a Group I metal carbonate, added to gelling systems initially catalyzed by either a different Group I, or Group II, metal carbonate was also studied. Secondary addition occurred at various times throughout the gelation process, and in such quantities as to give fixed R/C compositions across the range of catalyst combinations used. The gelation process was monitored using DLS, with final gels characterized using low temperature nitrogen sorption measurements, providing information on the textural properties of the samples prepared. The formation process and textural properties of the mixed catalyst systems could then be compared with typical RF gels, synthesized using a single Group I or Group II metal carbonate catalyst.

Experimental

Materials and Synthesis

Resorcinol (ReagentPlus, 99 %), aqueous formaldehyde solution (37 wt. % formaldehyde, stabilised with 10-15 % methanol), Na_2CO_3 (anhydrous, $\geq$ 99.5 %), cesium carbonate (Cs_2CO_3, ReagentPlus, 99 %), calcium carbonate ($CaCO_3$, $\geq$ 99 %) and barium carbonate ($BaCO_3$, ACS reagent $\geq$ 99 %) were used as purchased from SigmaAldrich UK.

RF solution compositions were determined by fixing the molar ratio of resorcinol to formaldehyde (R/F) at 0.5, the total solution volume at 60 mL and the total solids content at 20 % weight by volume, resulting in a constant solids mass of 12 g. As the R/C and chosen

metal carbonate changed, the individual masses of R, F and C were adjusted, accordingly, to maintain a total solids mass of 12 g. All preparations were carried out at room temperature.

For gels made using single Group II metal carbonate catalysts, R/C values of 100 and 200 were used. For mixed systems with two metal carbonate catalysts, these were combined in a molar ratio of 50:50. The initial system was prepared with an R/C ratio of 200, which following the addition of the secondary catalyst (also at R/C 200), resulted in an overall R/C of 100.

For reactions using either a single carbonate catalyst, or simultaneous addition of two carbonate catalysts, the required mass of resorcinol was completely dissolved in 50 mL of deionised water (Millipore Elix 5) in a 500 mL sealable jar under magnetic stirring. The appropriate mass of carbonate(s) was added to this solution with continued stirring until complete dissolution was again achieved. As both calcium and barium carbonate have very low solubilities in water,[16, 26, 27] complete dissolution was not possible, even with the small quantities used. These solutions were, therefore, left to stir for 5 minutes before proceeding. The required volumes of formaldehyde solution and additional deionised water were added to the jar to give a total volume of 60 mL. The reaction vessel was sealed and allowed to stir continuously for 30 min, after which it was transferred to a preheated oven set to 85 ± 5 °C until gelation occurred. Gelation times were monitored by periodically tilting the jars to an angle of 45° until no flow was observed. The gels were left to cure in the oven, with the temperature maintained at 85 ± 5 °C.

The production of gels utilising the secondary addition of metal carbonate required a modification to the synthesis procedure described above. Resorcinol and the primary carbonate were dissolved in 40 mL of deionised water, while the other 10 mL was used to dissolve the secondary metal carbonate in a second, smaller vial. Formaldehyde and

142 additional water were added as before, to the resorcinol/primary carbonate mixture, and the
143 RF solution stirred for 30 min. The sample was placed in the oven (85 ± 5 °C) along with the
144 secondary carbonate solution container. At a predetermined point during the gelation process
145 of the RF system, both containers were removed from the oven and the secondary carbonate
146 solution added to the main RF reaction jar. The mixture was stirred for 30 seconds to ensure
147 thorough mixing and then returned to the oven to complete the gelation and curing steps.

148 After remaining in the oven to gel and cure for a further 3 d, the gels were removed and
149 allowed to cool. The aqueous pore liquid was exchanged for acetone by shaking the sample in
150 180 mL of acetone (ACS reagent, ≥ 99.5%, SigmaAldrich) for 3 d at room temperature. The
151 samples were finally dried under vacuum for 2 d at 85 °C to produce the xerogel product.

152 **Xerogel Characterisation**

153 Each dried xerogel was characterised using nitrogen sorption measurements (Micromeritics
154 ASAP 2420) in order to determine surface area and porosity. Approximately 0.5 g of the
155 dried xerogel was first degased under vacuum at 110 °C for 2 h in order to remove any
156 residual solvent or other contaminants from the material surface; analysis was performed at -
157 196 °C, maintained through the use of liquid nitrogen, and consisted of 40 point adsorption
158 and 30 point desorption cycles.

159 The resulting nitrogen uptake isotherms were analysed using Brunauer-Emmett-Teller (BET)
160 theory,[28] applied to the adsorption branch: a linear plot analysed using relative pressures
161 (p/p_0) in the range 0.05 and 0.3, allowed for the calculation of the BET surface area (S_{BET}).
162 Pore size distributions were determined using the Barrett-Joyner-Halenda (BJH) method,[29]
163 applied to the desorption branch, which also allowed calculation of average (mean) pore
164 sizes. It is known that the pores within these RF materials are not cylindrical, and the BJH
165 model cannot, therefore, strictly be applied to calculate the size of pores detected. However,

no other practical method of pore size determination is available, and use of the BJH method is prevalent throughout the literature with respect to RF gel pore size determination.

Dynamic Light Scattering

All DLS measurements were performed on an ALV/CGS-3 compact goniometer and ALV/LSE-5004 multiple tau digital correlator. Measurements were taken using a laser wavelength, λ, of 632.8 nm and a scattering angle, θ, of 90°.

Samples prepared using either a single metal carbonate or simultaneous addition of two metal carbonates were analysed using the same experimental procedure. 11 equal portions of the RF solution, prepared as per the method outlined above, were passed through a 0.2 μm pore size PTFE syringe filter (Whatman Puradisc) into separate borosilicate glass cells (10 mm diameter, 75 mm height, Fisher Scientific). Each cell was sealed with a cap, and 10 were placed in an oven at 85 ± 5 °C. The remaining cell, designated t = 0, was analysed immediately. Subsequent cells were removed from the oven after an appropriate time interval, whereupon they were rapidly quenched to 22 °C in a climate controlled room.

Samples produced using secondary addition of carbonate required a modification to the analysis procedure. Before secondary addition, the primary carbonate solution was analysed as described above. Post addition, small volumes of the newly mixed solution were transferred into further glass cells and returned to the oven, before removal, quenching and analysis, as before, at appropriate time intervals.

Autocorrelation functions of the scattered light intensities were measured for each sample and the cumulant method[30] was applied to each autocorrelation function to determine the initial decay rate, $\Gamma(s^{-1})$. The mean diffusion coefficient, D, was subsequently calculated using:

$$\Gamma = Dq^2$$

where q is the scattering vector magnitude.

$$q = \frac{4\pi n_0}{\lambda} sin\frac{\theta}{2}$$

where n_0 is the refractive index. The Stokes-Einstein[31, 32] equation could then be used to calculate the mean hydrodynamic radius, R_H:

$$R_H = \frac{k_b T}{6\pi\mu D}$$

where k_B is the Boltzmann constant, T is absolute temperature and μ is the dynamic viscosity. For all calculations, μ was assumed to be that of pure water at the experimental temperature of 22 °C (8.9×10^{-4} Pa.s).

Results and Discussion

Gelation times were determined for gels synthesized using either a single metal carbonate, or the simultaneous addition of two metal carbonates, making use of the tilt method. Gels were checked periodically in the initial stages of reaction, and then every 30 s as gelation approached, as indicated by a visible increase in viscosity. Samples were said to have gelled when no flow was detected when sitting at a 45° angle. These newly determined values were then compared with those previously obtained for gels made with Group I metal carbonates. It was found that, for an equivalent R/C, both $CaCO_3$ and $BaCO_3$ exhibited equal gelation times: 40 min for R/C 100 and 45 min for R/C 200. Furthermore, it was found that simultaneous combination of Cs_2CO_3 and Na_2CO_3, both Group I catalysts, with a total R/C of 100, gave a gelation time of 35 min – identical to those of the individual metal carbonates.[8]

Combination of either Group II metal carbonate with Na_2CO_3 resulted in a consistent gelation time of 40 min.

These gelation times were used to define appropriate interval times for the DLS measurements. To allow for direct comparison between samples after an equivalent fraction of gelation time had passed, intervals were set at 10 % of the total gel time, e.g. a gelation time of 40 min corresponded to intervals of 4 min. As such, an equal number of measurements were obtained for each sample.

Group II metal carbonate catalysts

Figure 1 shows normalized autocorrelation functions obtained for samples representative of the entire gelation period for $CaCO_3$ at R/C 100. It can be seen that all but the final decay profiles follow an exponential dependence on time, indicative of free Brownian motion of primary clusters within these samples. The final profile, i.e. t = 100 %, exhibits nonergodicity, which implies that the gel has a large degree of permanent structure, as would be expected at the time corresponding to gelation. Autocorrelation functions for the Group II catalyzed samples display no secondary decay, unlike the autocorrelation functions displayed by Group I catalysts (an example of which is reproduced from Taylor *et al*.[8] in the S.I.). Secondary decays are indicative of networking and aggregation of primary clusters occurring later in the gelation formation process. Instead, for Group II catalysts, primary clusters appear to grow unhindered to larger sizes, as supported by visual inspection of the samples during gelation. When a Group II catalyst was used, turbidity was observed in the latter stages of gelation, which is indicative of larger primary cluster sizes being present in the analyzed sample. In contrast, Group I catalyzed samples remained transparent throughout gelation, including the networking and aggregation stages.

Cumulant analysis was applied to all autocorrelation functions corresponding to non-turbid samples, in order to determine hydrodynamic radii of primary clusters. Turbidity results from a high optical contrast, which, in turn, leads to multiple scattering of the light and prevents accurate calculation of hydrodynamic radii. Figure 2 shows the hydrodynamic radii, as determined from the initial decay of the autocorrelation functions.

It can be seen that all four Group II metal carbonate catalyst samples exhibit primary cluster sizes that fall into a narrow overlapping band, in a manner similar to the results previously obtained for Group I carbonates (Li, Na and K).[8] However, the radii obtained here are much larger than those observed for the Group I catalysts. It is worth noting that, despite the difference in R/C ratio, the maximum observed hydrodynamic radius obtained is very similar in each case. This is in contrast to the results for the Group I catalysts, where increasing R/C lead to an increase in observed maximum cluster size. However, the limited water solubility of the Group II carbonates must be taken into account. With water solubilities of 0.0015 g/100 ml and 0.00141 g/100 ml at 25 °C for calcium and barium carbonate respectively,[33] at the catalyst concentrations used for these samples, the saturation limit is far exceeded, with the remaining undissolved solid remaining as visible sediment within the reaction vessel. During filtration prior to DLS analysis, any undissolved catalyst particles larger than the 0.2μm filter pore size will be removed from the system and in turn, it is unlikely any smaller particles are passing through the filter, as these would be clearly visible in the autocorrelation functions acquired. As such, for a given catalyst, the analyzed samples are likely to be a saturated solution of equivalent catalyst concentration, irrespective of the initial R/C chosen. Nevertheless, the increased cluster size, in conjunction with the lack of secondary decay, supports the theory that rather than aggregating and networking during the gelation phase, primary clusters grow continuously to larger sizes until the critical gelation volume fraction is

252 reached and the gel is formed. The curing phase sees cross-linking and networking into a
253 solid 3D framework.

254 Figure 3 shows both the adsorption/desorption isotherms and pore size distributions for the
255 Group II metal carbonate catalyst samples. The N_2 isotherms show considerably greater
256 uptakes than those previously observed for Li, Na and K carbonate at the corresponding R/C
257 ratio.[8] While the uptakes for Cs_2CO_3 are closer to those of the Group II metal carbonate
258 catalysts, the increase is still significant. Average pore sizes follow a similar trend to the
259 Group I catalyst systems, increasing as the added catalyst concentration is reduced.
260 Congruent with the N_2 uptakes, the average pore sizes are also much larger in the presence of
261 a Group II metal carbonate when compared to the Group I analogues. As the pores within an
262 RF gel network are comprised of the gaps between clusters, the larger pores provide further
263 evidence that clusters grow to much larger sizes, pack less tightly, and result in larger
264 intercluster voids for the Group II catalyzed samples.

265 These pore size results are in contrast to the cluster sizes observed during DLS
266 measurements. However, there may be a number of factors to explain why this is the case. As
267 previously explained, the samples grew turbid as the heating times increased and, as such, it
268 was not possible to continue to analyze samples using DLS past this point. It is entirely
269 possible that the clusters continue to grow beyond the final sizes observed, resulting in
270 different structures and correspondingly different pore sizes. Additionally, the remaining
271 catalyst present may play a complex role in the final structure formation. The ever changing
272 conditions within the reaction vessel are likely to alter the solubility of the catalysts, with it
273 being known that increased temperature adversely affects the solubility.[26, 27] Combined with
274 the proceeding reaction between R and F, the levels of Ca^{2+} or Ba^{2+} cations may well differ
275 depending on initial R/C, resulting in the differences in pore sizes that are observed.

Table 1 outlines the textural properties obtained from the N_2 sorption isotherms, showing the BET surface area (S_{BET}), total pore volume (V_{Tot}), the micropore volume (V_{μ}) and the average pore size (d_p avg.). The differences between the Group I and Group II carbonate catalysts are clear. The greatly increased pore sizes obtained when using a Group II carbonate leads to a corresponding increase in pore volume, as well as a significant decrease in the measured surface area.

Secondary addition of catalyst

Table 2 outlines the three metal carbonate combinations studied in this work. Each combination consists of a primary carbonate, added initially, and a secondary carbonate, added to the initial system after a predetermined time. Due to the marked differences between samples prepared using Cs_2CO_3 and the other Group I carbonates, it was chosen as a primary carbonate along with Group II carbonates. Na_2CO_3 was picked as the representative of the other Group I species, due to the similarities between samples prepared with Li, Na or K as cation, and so became the secondary carbonate. This produced combinations of either two M^+ cations or both an M^+ and M^{2+} cation.

Figure 4 shows the hydrodynamic radii obtained for each combination of primary cation when mixed with Na_2CO_3 at the selected time interval. Due to the development of secondary decays for Cs_2CO_3 samples, and turbidity effects for $CaCO_3$ and $BaCO_3$ samples, only experimental runs with simultaneous addition, and addition at 60 % of the primary gel time, yielded accurate hydrodynamic radii data. Other additions before 60% of the gelation time had passed were not conducted, due to the lack of cluster growth observed at shorter times.

Figure 4a details the results of the combined Cs_2CO_3/Na_2CO_3 systems. It is clear to see how different the cluster sizes are when using solely Na_2CO_3 or Cs_2CO_3 as the catalyst, with the Cs_2CO_3 cluster size greatly exceeding that of the Na_2CO_3 catalyzed clusters. With

simultaneous addition of these two catalysts, cluster sizes fall directly between those observed for the single catalyst systems, with both catalysts playing a role in the cluster formation process. In contrast, delayed addition of Na_2CO_3 at 60% shows a much altered growth profile. In the initial stages, i.e. before secondary addition, cluster growth follows that of the Cs_2CO_3 catalyzed system, as would be expected. However, immediately post addition there is a significant decrease in the observed cluster size. This is followed by limited regrowth of the clusters before the onset of networking and aggregation. Secondary addition is, therefore, causing a marked modification of the gelation process.

Both the $CaCO_3/Na_2CO_3$ and $BaCO_3/Na_2CO_3$ mixed systems exhibit comparable results, with noticeable differences to the Cs_2CO_3/Na_2CO_3 system. In the case of simultaneous addition of the two catalysts, cluster sizes closely follow those of a pure Na_2CO_3 system at R/C 200. This corresponds to the concentration of Na_2CO_3 present in the mixed catalyst system, suggesting that it plays a dominant role during gelation, with the Group II catalyst having very little influence on the process. With delayed addition of the Na_2CO_3, pre-addition cluster growth again follows the growth profile exhibited by the primary carbonate catalyst. On addition of the Na_2CO_3 there is a reduction in cluster size, however, this is not as significant as that witnessed with the Cs_2CO_3/Na_2CO_3 system. Following addition, the clusters again regrow, with the size reached before networking and aggregation being comparable to those seen immediately prior to addition. It is also clear that delayed addition of Na_2CO_3 to any of the primary catalyst systems results in final cluster sizes much smaller than those observed through the use of just the primary catalyst, approximately halving in the case of Cs_2CO_3 and falling to almost one third for the Group II catalysts. This suggests that the Na_2CO_3 is again playing a dominant role in the formation of these RF gels.

Further evidence of the dominance of the Na_2CO_3 on cluster growth can be seen from the autocorrelation functions, in particular those of the $CaCO_3$ and $BaCO_3$ systems. Where the

single Group II metal carbonate systems show no secondary decay as gelation is approached (Figure 1), addition of the Na_2CO_3 to the system causes secondary decays to once more develop near gelation, as was observed for all single Group I catalyst samples. An example set of Group II/Group I secondary addition autocorrelation functions are given in the S.I. Close examination of the autocorrelation functions also reinforces the interpretation of cluster size decreasing on addition of Na_2CO_3. DLS measures the average size of clusters, such that the introduction of an additional new species of small cluster would cause a reduction in the average cluster size. However, the profile of the first post-addition sample maintains a purely exponential decay, indicative of a predominantly monodisperse sample of smaller clusters. An example of this monodispersity is shown in the S.I.

Figures 5 and 6 show the nitrogen sorption isotherms, and pore size distributions, respectively, obtained for the three primary catalysts with secondary addition of sodium carbonate simultaneously, and at 60, 70 and 80 % of the primary gel time. Single catalyst data for primary and secondary species are once more included for reference. Analysis of this data further reinforces the dominant role of Na_2CO_3 during gel formation. As can be seen from Figure 5, there is a distinct clustering of the isotherms for all of the systems, centering on that of Na_2CO_3 at R/C 200. Only addition at 80 % of the primary gel time does the isotherm deviate from this clustering, moving closer to that of the primary system. This change results in greater nitrogen uptake and shifting of the hysteresis loop to higher relative pressures, indicating an increase in both average pore size and total pore volume. The pore size distributions obtained (Figure 6) back up these observations, with the distributions for simultaneous, 60 % and 70 % addition again grouped around those of the Na_2CO_3 gels. Meanwhile, addition at 80 % gives rise to larger average pore sizes.

Table 3 provides further textural properties of the mixed catalyst systems, again consisting of S_{BET}, V_{Tot}, V_{μ} and d_p *avg*. The data shows how simultaneous, 60 % and 70% addition samples

350 can be grouped in terms of surface area, pore volume and average pore size, with values
351 comparable to those of the pure Na_2CO_3 gels as opposed to those of their respective primary
352 catalyst. As was the case for the isotherms and pore size distributions, samples with addition
353 at 80 % of the primary gel time show meaningful differences in these properties, with
354 increased average pore size and decreased surface area, that while still greatly different, move
355 the properties of the 80 % gels closer to the primary samples.

356 As a reference, secondary addition of Na_2CO_3 to a parent Na_2CO_3 gel was also performed, to
357 further examine the interactions between metal carbonate additions. The results for these
358 systems can be found in the Supplementary Information. In this case, there is very little
359 difference in the properties of the gels, irrespective of when the secondary addition is carried
360 out.[34] However, this is not unexpected, as the catalyst combination effectively transforms the
361 initial Na_2CO_3 R/C 200 system into a R/C 100 system, and the properties follow this trend,
362 being highly similar to those of a conventionally produced R/C 100 gel.

363 Collective consideration of these results shows potential routes towards tuning the pore size
364 of the xerogels, while keeping the total ionic strength constant. This contrasts with the most
365 common method of inducing such control, i.e. altering the R/C ratio. Constant ionic strength
366 may be of importance in situations such as incorporating biological elements into the gel
367 structure that would be sensitive to change. Furthermore, the gels demonstrating similar
368 average pore sizes and total pore volumes to those of the sodium carbonate catalyzed gels
369 display much narrower distributions. This implies less disperse porosity, with more pores of
370 the same size, making the material more ordered.

371 The average pore sizes obtained in this work contrast with the study of Feng *et al.*,[23] who
372 observed an increase in average pore size and widening of the pore size distribution on
373 secondary base addition. The Dollimore-Heal method[35] used by Feng *et al*.[23] to calculate their

pore size distribution should be comparable to the BJH model in all but only slight details of the mathematics; as such, the two methods should give comparable results. It is well established that an increase in catalyst concentration will cause a decrease in average pore size, which supports the results presented here and indicating other factors may have affected the materials produced by Feng *et al*.[23]

Nevertheless, the secondary addition results here show that, even at times approaching 80 % of the initial primary gel time, when cluster growth is significant, and structure formation is well underway in the case of Cs_2CO_3, it is still possible to manipulate these processes to a significant degree. This suggests that even at this time there is still free unreacted material (be it resorcinol, formaldehyde, hydroxymethyl derivatives or oligomeric chains) available to participate in the reaction and contribute to the gel network. This is especially the case of Cs_2CO_3 as the primary cation. Previous work has established that, by 70 % of the gel time, aggregation and networking of primary clusters has begun. Even so, the addition of Na_2CO_3 during this period is still capable of disrupting the process to a discernible degree, forcing reorganization of the structure before the irreversible cluster aggregation can be completed. However, by 80 % of the gel time, aggregation of primary clusters is well established, and the process is more difficult to disrupt, giving gel properties closer to the initial primary catalyst gel than the other combinations studied. This apparent reversibility provides evidence that the primary clusters are not composed of a single oligomeric/polymeric molecule or chain. As the introduction of a salt would not cause the breakdown of these polymerized species, there must be a degree of physical interaction between multiple chains, which in turn form the clusters. When the new salt is added, these physical interactions are disrupted; the chains are rearranged in solution and the observed cluster size changes.

In a previous study,[8] we have proposed a Hofmeister like series placing the four Group I metal cations used in order, relative to the average size of RF cluster produced by each system, such that:

$$Li \approx Na \approx K < Cs$$

From the results presented in this work, we can expand this series to include the newly acquired data from Group II metal cations, and their respective cluster sizes:

$$Li \approx Na \approx K < Cs < Ca \approx Ba$$

Compared with the established Hofmeister series, Cs appears out of position.[36] The Hofmeister series was developed according to the interactions between the various cations and protein molecules in aqueous solution. The RF oligomers that form during gelation will be large and complex macromolecules with both hydrophobic and hydrophilic regions, therefore, the interactions with the various cations may qualitatively be similar to the proteins studied during development of the Hofmeister series. Cations with high charge densities (i.e. small cations with a large charge, e.g. Ca^{2+}) lead to a disruption of the hydration layer around the protein molecule, leading them to be salted out. In contrast, low charge density cations (large cations with a small charge, e.g. Cs^{+}) can enhance the hydration layer and keep the proteins dispersed in solution. As a result, it would be expected that Cs would produce the smallest clusters of any of the cations studied.

However, it may be that these small clusters are actually forming, but their presence is disguised. The rapid increase in cluster size observed for Cs_2CO_3 catalyzed systems may be indicative of coalescence or a self-assembly mechanism of smaller clusters. Much larger than expected clusters would therefore be seen using DLS. This observation is supported by the secondary addition of Na_2CO_3 as studied in this work. When Cs_2CO_3 and Na_2CO_3 are added

simultaneously, the presence of the Na cation results in larger initial cluster sizes, and the rapid size increase of the clusters coming together is not witnessed. Similarly, when the Na_2CO_3 is added during gelation, the Na starts to interact with the clusters. The many oligomers that compose the clusters are again unlikely to be chemically bound, and the interactions between the oligomers and the surrounding environment will change, resulting in the clusters rearranging into smaller individual units.

In the case of both $CaCO_3$ and $BaCO_3$ the increased charge density imparted by the 2+ charge disrupts the hydration layer surrounding the RF oligomers. This leads to hydrophobic interactions and loose packing of these oligomers into clusters. As a result, cluster sizes are larger than those observed for the Group I catalysts. By introducing Na_2CO_3 into the system, cation-oligomer interactions are altered and this appears to restore the hydration layer to some extent. Simultaneous addition then indicates that the layer is not disrupted, and the clusters, therefore, have size similar to those if only the Na were present. With delayed addition, the hydration layer is initially disrupted, leading to the loosely packed oligomers. However, on addition of the Na_2CO_3, the hydration layer is partially restored, reducing the hydrophobic effect and allowing the oligomers to pack more tightly. As a result, the size of the clusters decreases and the newly added Na prevents further growth to very large sizes, giving final cluster sizes much smaller than those expected with just the Group II catalysts.

It can also be considered that the cations present within the system can be classified as Lewis acids. According to Pearson's theory of hard and soft acids and bases, both Na^+ and Ca^{2+} can be classified as hard acids, while Cs^+ is a soft acid.[37] Likewise, regions of the newly formed oligomers can be similarly classified, with hydroxyl groups being hard bases, and aromatic rings being soft bases.[37] As 'like prefers like' with regards to these species, it is possible that the different cations will interact differently with the oligomers, influencing their structure, and consequently, their size. This would go some way to explaining the disparity between

445 gels containing Na and Cs. However, as both Na^+ and Ca^{2+} are both hard acids, it cannot fully
446 explain the vast differences in formation and structure observed for these systems.
447 Nevertheless, this cluster growth process can be depicted schematically, as shown in Figure
448 7. For clarity, the clusters are depicted as spherical as the exact shape and internal structure of
449 the clusters is not yet known.

450 By controlling the interaction between the RF oligomers and the cations present it is,
451 therefore, possible to control the final pore size in dried xerogels, while maintaining a
452 constant R/C and therefore constant ionic strength. Additionally, the narrowing of the pore
453 size distribution, indicative of more ordered materials, resulting from using mixed catalysts
454 may be highly advantageous for the applications of RF xerogels, e.g. in gas separation
455 processes.

456 **Conclusions**

457 Gels were prepared using a mixture of two catalysts; a primary metal carbonate chosen from
458 caesium, calcium or barium carbonate, and a secondary carbonate, the choice being sodium
459 carbonate. The latter was added at various time intervals within the primary carbonate
460 gelation period, and gels were analysed using DLS, in conjunction with textural
461 measurements to monitor the changes induced by differing catalyst combinations and
462 addition times. Equal concentrations of both primary and secondary carbonates, i.e. a 50:50
463 molar ratio, were used for all combinations. With a Group II carbonate and sodium carbonate,
464 simultaneous addition gave primary cluster sizes congruent with only the sodium carbonate
465 being present at all times, with delayed addition of the sodium carbonate resulting in
466 significant reduction in size of primary clusters upon addition of the secondary carbonate. In
467 almost all cases, the textural properties of the dried gel reflected those of the corresponding
468 sodium carbonate gel prepared with half the total catalyst content (i.e. R/C 200). Only

addition of the secondary carbonate at 80% of the parent gel time resulted in significantly modified properties, with an increase in pore diameter, as there was little unreacted material with which to form clusters, resulting in larger intercluster voids and correspondingly larger pores. By contrast, an equal molar ratio of caesium and sodium carbonates produced intermediate cluster sizes on simultaneous addition, while delayed addition of sodium carbonate once again resulted in significant reduction of size of the primary clusters. These results indicate that it is possible, by careful selection of the catalyst combination, and addition time, to fine tune the porous texture of RF xerogels. We note that this can be achieved while also maintaining total ionic strength, which is important for key applications, especially involving biological systems, such as bone scaffolding.[38] Overall, the small average pore sizes associated with high concentrations of sodium carbonate can be retained while narrowing the pore size distribution, resulting in greater regularity of the structure, while increasing the total pore volume of the system.

ASSOCIATED CONTENT

Supporting Information. Hydrodynamic radii for both Na_2CO_3 and Cs_2CO_3 at R/C 100 and 200, DLS autocorrelation functions for delayed addition of Na_2CO_3 to a $CaCO_3$ catalyzed system and N_2 sorption isotherms, pore size distributions and textural properties for delayed addition of Na_2CO_3 to a Na_2CO_3 catalyzed system (PDF). This material is available free of charge via the Internet at http://pubs.acs.org.

AUTHOR INFORMATION

Corresponding Author

*E-mail: ashleigh.fletcher@strath.ac.uk.

Notes

The authors declare no competing financial interest.

ACKNOWLEDGEMENTS

The authors acknowledge financial support from the University of Strathclyde for SJT.

ABBREVIATIONS

R, resorcinol; F, formaldehyde; C, catalyst; R/C, resorcinol to catalyst molar ratio; R/F, resorcinol to formaldehyde molar ratio; DLS, dynamic light scattering; BET, Brunauer-Emmett-Teller; BJH, Barrett-Joyner-Halenda; DH, Dollimore-Heal

REFERENCES

(1) Rodrigues, E. G.; Pereira, M. F. R.; Órfão, J. J. M. Glycerol oxidation with gold supported on carbon xerogels: Tuning selectivities by varying mesopore sizes. *Applied Catalysis B: Environmental* **2012**, *115–116*, 1-6.

(2) Zubizarreta, L.; Menéndez, J. A.; Job, N.; Marco-Lozar, J. P.; Pirard, J. P.; Pis, J. J.; Linares-Solano, A.; Cazorla-Amorós, D.; Arenillas, A. Ni-doped carbon xerogels for H2 storage. *Carbon* **2010**, *48*, 2722-2733.

(3) Yamamoto, T.; Endo, A.; Ohmori, T.; Nakaiwa, M. Porous properties of carbon gel microspheres as adsorbents for gas separation. *Carbon* **2004**, *42*, 1671-1676.

(4) Petričević, R.; Glora, M.; Fricke, J. Planar fibre reinforced carbon aerogels for application in PEM fuel cells. *Carbon* **2001**, *39*, 857-867.

(5) Pekala, R. W. Organic aerogels from the polycondensation of resorcinol with formaldehyde. *Journal of Materials Science* **1989**, *24*, 3221-3227.

(6) Jin, H.; Zhang, H.; Ma, Y.; Xu, T.; Zhong, H.; Wang, M. Stable support based on highly graphitic carbon xerogel for proton exchange membrane fuel cells. *Journal of Power Sources* **2010**, *195*, 6323-6328.

(7) Pekala, R. W.; Kong, F. M. A synthetic route to organic aerogels - mechanism, structure and properties. *Journal De Physique* **1989**, *50*, 33-40.

(8) Taylor, S. J.; Haw, M. D.; Sefcik, J.; Fletcher, A. J. Gelation Mechanism of Resorcinol-Formaldehyde Gels Investigated by Dynamic Light Scattering. *Langmuir* **2014**, *30*, 10231-10240.

(9) Al-Muhtaseb, S. A.; Ritter, J. A. Preparation and Properties of Resorcinol-Formaldehyde Organic and Carbon Gels *Journal of Advanced Materials* **2003**, *15*, 101-114.

(10) El Khatat, A. M.; Al-Muhtaseb, S. A. Advances in Tailoring Resorcinol-Formaldehyde Organic and Carbon Gels. *Advanced Materials* **2011**, *23*, 2887-2903.

(11) Merzbacher, C. I.; Meier, S. R.; Pierce, J. R.; Korwin, M. L. Carbon aerogels as broadband non-reflective materials. *Journal of Non-Crystalline Solids* **2001**, *285*, 210-215.

(12) Brandt, R.; Petricevic, R.; Pröbstle, H.; Fricke, J. Acetic Acid Catalyzed Carbon Aerogels. *Journal of Porous Materials* **2003**, *10*, 171-178.

(13) Job, N.; Gommes, C. J.; Pirard, R.; Pirard, J.-P. Effect of the counter-ion of the basification agent on the pore texture of organic and carbon xerogels. *Journal of Non-Crystalline Solids* **2008**, *354*, 4698-4701.

(14) Fairén-Jiménez, D.; Carrasco-Marín, F.; Moreno-Castilla, C. Porosity and surface area of monolithic carbon aerogels prepared using alkaline carbonates and organic acids as polymerization catalysts. *Carbon* **2006**, *44*, 2301-2307.

(15) Anderson, L. The Effect of the Catalyst on the Formation of RF Xerogels. PhD, University of Strathclyde2014.

(16) Taylor, S. J. Monitoring the Gelation Mechanism of Resorcinol-Formaldehyde Xerogels. PhD, University of Strathclyde2014.

(17) Job, N.; Pirard, R.; Marien, J.; Pirard, J.-P. Porous carbon xerogels with texture tailored by pH control during sol–gel process. *Carbon* **2004**, *42*, 619-628.

(18) Job, N.; Panariello, F.; Marien, J.; Crine, M.; Pirard, J.-P.; Léonard, A. Synthesis optimization of organic xerogels produced from convective air-drying of resorcinol–formaldehyde gels. *Journal of Non-Crystalline Solids* **2006**, *352*, 24-34.

(19) Mulik, S.; Sotiriou-Leventis, C.; Leventis, N. Time-Efficient Acid-Catalyzed Synthesis of Resorcinol−Formaldehyde Aerogels. *Chemistry of Materials* **2007**, *19*, 6138-6144.

(20) Lin, C.; Ritter, J. A. Effect of synthesis pH on the structure of carbon xerogels. *Carbon* **1997**, *35*, 1271-1278.

(21) Lambert, S. M.; Overturf, G. E.; Wilemski, G.; Letts, S. A.; Schroen-Carey, D.; Cook, R. C. Fabrication of low-density foam shells from resorcinol-formaldehyde aerogel. *Journal of Applied Polymer Science* **1997**, *65*, 2111-2122.

(22) Laskowski, J.; Milow, B.; Ratke, L. Subcritically dried resorcinol-formaldehyde aerogels from a base-acid catalyzed synthesis route. *Microporous and Mesoporous Materials* **2014**, *197*, 308-315.

(23) Feng, Y. N.; Miao, L.; Tanemura, M.; Tanemura, S.; Suzuki, K. Effects of further adding of catalysts on nanostructures of carbon aerogels. *Materials Science and Engineering: B* **2008**, *148*, 273-276.

(24) Yamamoto, T.; Yoshida, T.; Suzuki, T.; Mukai, S. R.; Tamon, H. Dynamic and static light scattering study on the sol-gel transition of resorcinol-formaldehyde aqueous solution. *Journal of Colloid and Interface Science* **2002**, *245*, 391-396.

(25) Gaca, K. Z.; Sefcik, J. Mechanism and kinetics of nanostructure evolution during early stages of resorcinol–formaldehyde polymerisation. *Journal of Colloid and Interface Science* **2013**, *406*, 51-59.

(26) Coto, B.; Martos, C.; Peña, J. L.; Rodríguez, R.; Pastor, G. Effects in the solubility of $CaCO_3$: Experimental study and model description. *Fluid Phase Equilibria* **2012**, *324*, 1-7.

(27) Busenberg, E.; Plummer, L. N. The solubility of BaCO3(cr) (witherite) in CO2-H2O solutions between 0 and 90°C, evaluation of the association constants of BaHCO3+(aq) and BaCO30(aq) between 5 and 80°C, and a preliminary evaluation of the thermodynamic properties of Ba2+(aq). *Geochimica et Cosmochimica Acta* **1986**, *50*, 2225-2233.

(28) Brunauer, S.; Emmett, P. H.; Teller, E. Adsorption of gases in multimolecular layers. *J. Am. Chem. Soc.* **1938**, *60*, 309-319.

(29) Barrett, E. P.; Joyner, L. G.; Halenda, P. P. The Determination of Pore Volume and Area Distributions in Porous Substances. I. Computations from Nitrogen Isotherms. *Journal of the American Chemical Society* **1951**, *73*, 373-380.

(30) Finsy, R. Particle sizing by quasi-elastic light scattering. *Advances in Colloid and Interface Science* **1994**, *52*, 79-143.

(31) Stokes, G. G. On the Effect of the Internal Friction of Fluids on the Motion of Pendulums. *Transactions of the Cambridge Philosophical Society* **1851**, *9*, 8-106.

(32) Einstein, A. On the Movement of Small Particles Suspended in Stationary Liquids Required by the Molecular-Kinetic Theory of Heat. *Annalen der Physik* **1905**, *17*, 549-560.

(33) Ropp, R. C. Chapter 5 - Group 14 (C, Si, Ge, Sn, and Pb) Alkaline Earth Compounds. In *Encyclopedia of the Alkaline Earth Compounds*, Ropp, R. C., Ed.; Elsevier: Amsterdam, 2013, pp 351-480.

(34) McCall, E. Effects of Secondary Sodium Carbonate Addition on the Porous Structure of Resorcinol-Formaldehyde Organic Xerogels. MSci, University of Strathclyde2012.

(35) Dollimore, D.; Heal, G. R. An improved method for the calculation of pore size distribution from adsorption data. *Journal of Applied Chemistry* **1964**, *14*, 109-114.

(36) Hofmeister, F. About the science of the effect of salts. *Archiv for Experimentelle Pathologie und Pharmakologie* **1888**, *24*, 247-260.

(37) Pearson, R. G. Hard and Soft Acids and Bases. *Journal of the American Chemical Society* **1963**, *85*, 3533-3539.

(38) Rubenstein, D. A.; Lu, H.; Mahadik, S. S.; Leventis, N.; Yin, W. Characterization of the physical properties and biocompatibility of polybenzoxazine-based aerogels for use as a novel hard-tissue scaffold. *Journal of Biomaterials Science, Polymer Edition* **2012**, *23*, 1171-1184.

595 **List of Tables**

599 **List of Figures**

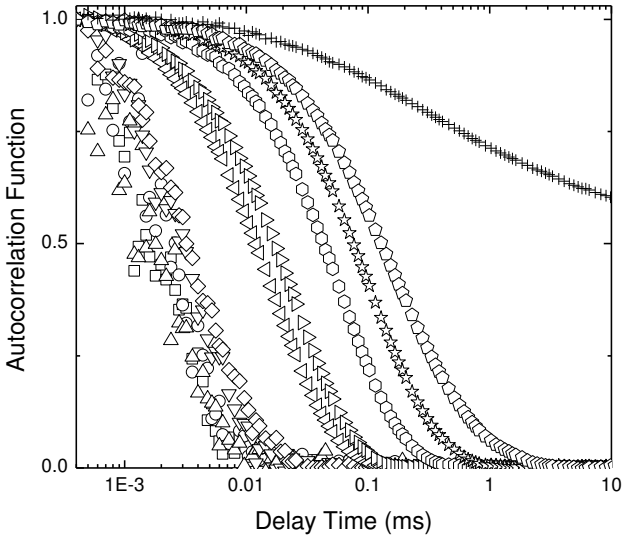

Figure 1. Normalized DLS autocorrelation functions for calcium carbonate at R/C 100. Measurements were taken every 10 % of the total gel time: (□) 0 %, (○) 10 %, (△) 20 %, (▽) 30 %, (◇) 40 %, (◁) 50 %, (▷) 60 %, (⬡) 70 %, (☆) 80 %, (⬠) 90 % and (+) 100 %.

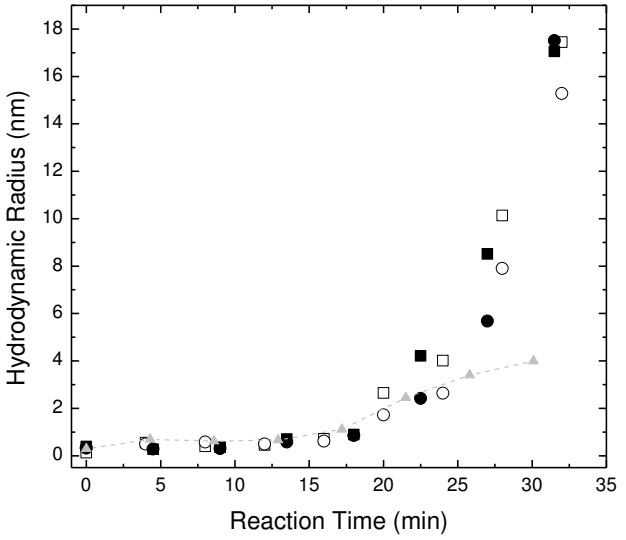

Figure 2. Mean hydrodynamic radii as determined from DLS autocorrelation functions for $CaCO_3$ at (□) R/C 100 and (■) R/C 200, and $BaCO_3$ at (○) R/C 100 and (●) R/C 200. Data for Na_2CO_3 at (▲) R/C 200 is included for comparison, with further comparative data included in the S.I. [8]

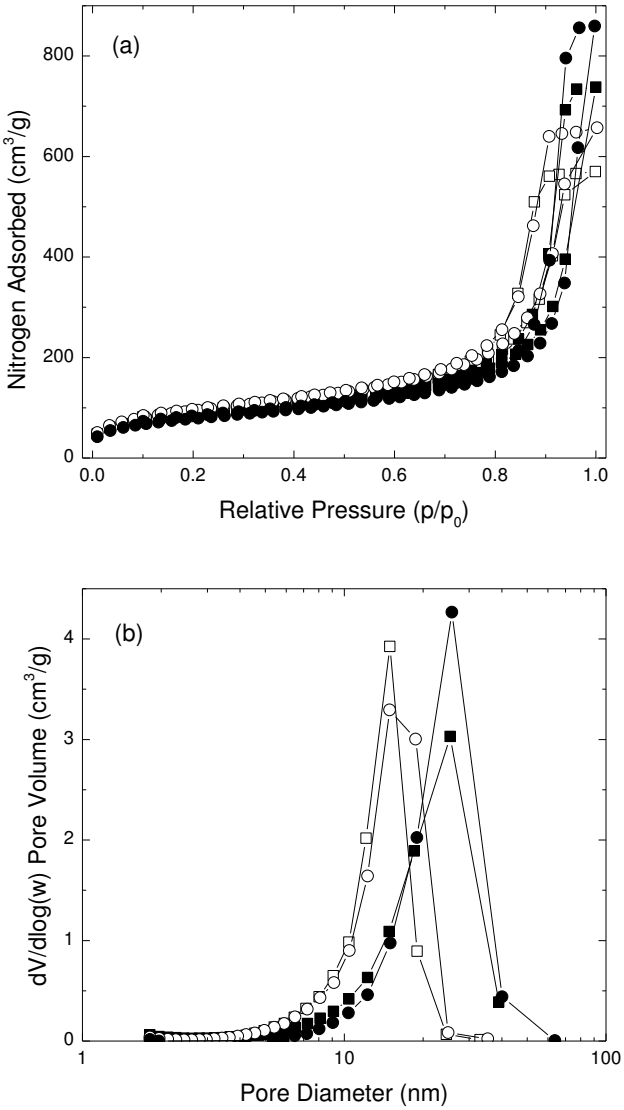

Figure 3. (a) N_2 sorption isotherms measured at -196 °C and (b) pore size distributions for calcium carbonate at (□) R/C 100 and (■) R/C 200 and barium carbonate at (○) R/C 100 and (●) R/C 200.

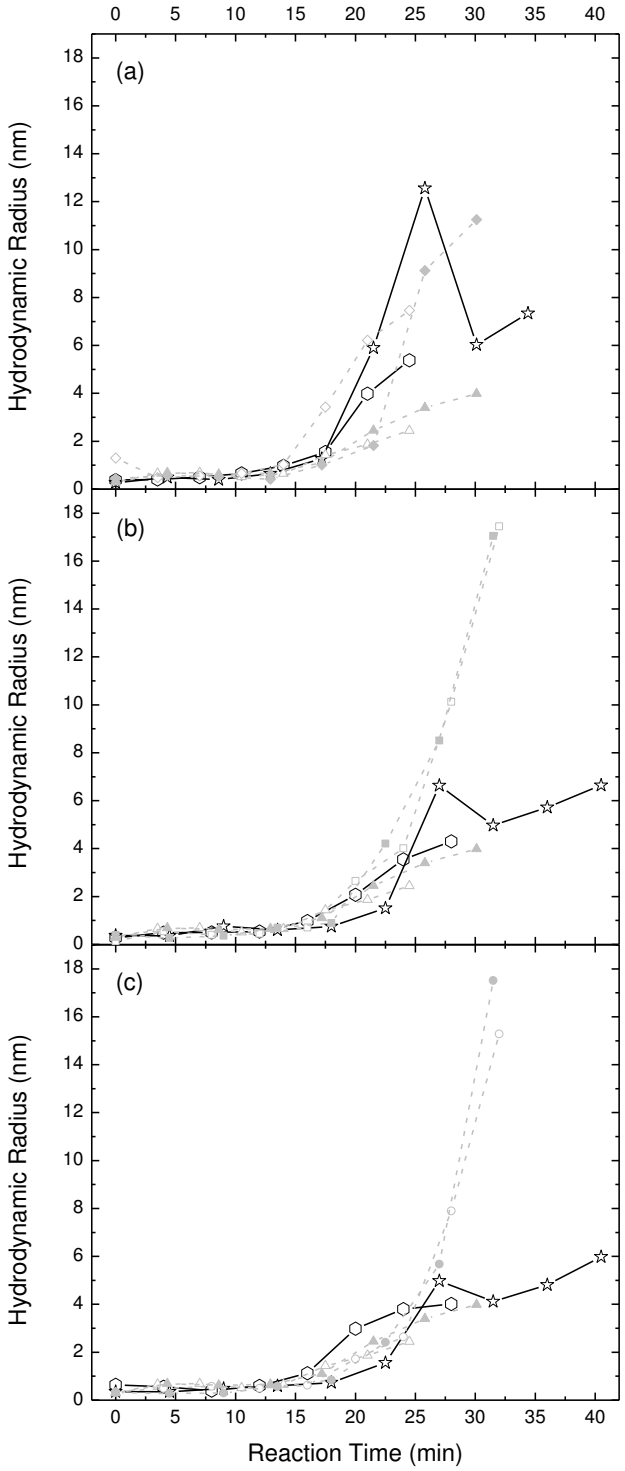

Figure 4. Mean hydrodynamic radii obtained using (a) Cs_2CO_3/Na_2CO_3, (b) $CaCO_3/Na_2CO_3$ and (c) $BaCO_3/Na_2CO_3$ at (⬡) simultaneous addition and (☆) secondary addition at 60%. Single catalyst data for (△) Na_2CO_3, (◇) Cs_2CO_3, (□) $CaCO_3$ and (○) $BaCO_3$ are reproduced for reference (open symbols R/C 100, and closed symbols R/C 200).

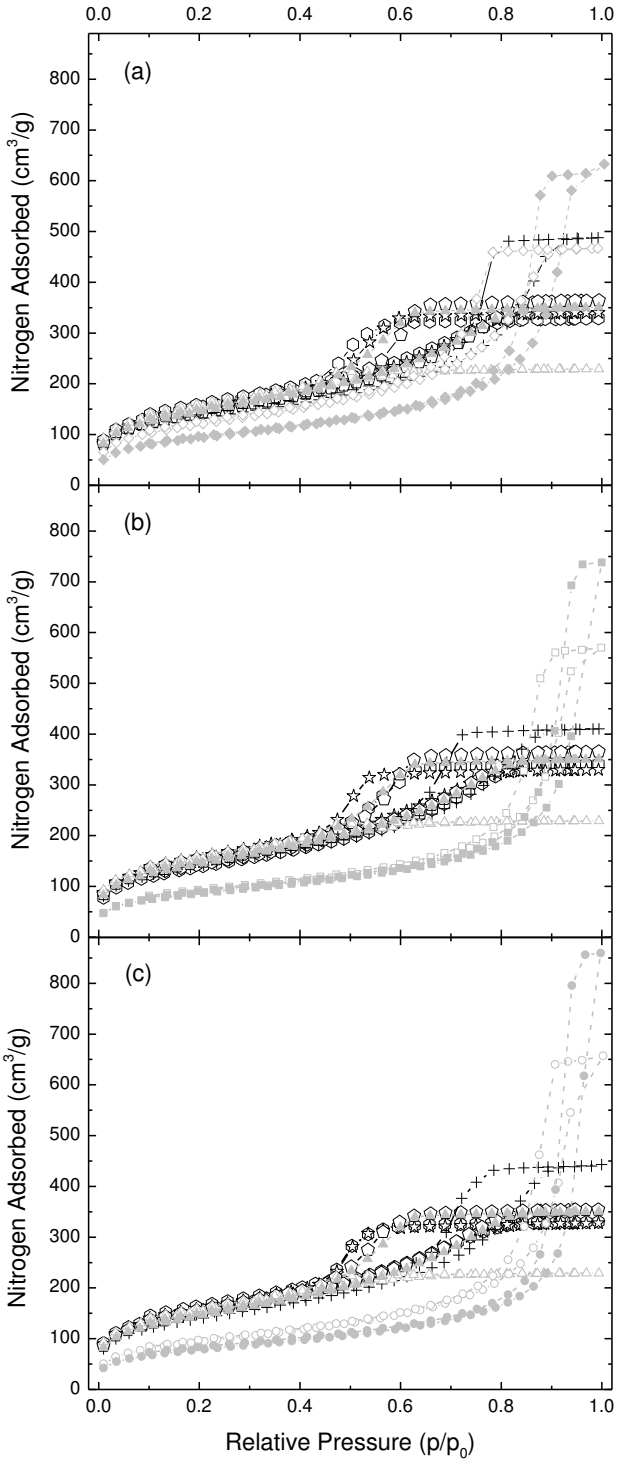

Figure 5. N_2 sorption isotherms measured at -196 °C for (a) Cs_2CO_3/Na_2CO_3, (b) $CaCO_3/Na_2CO_3$ and (c) $BaCO_3/Na_2CO_3$ at (⬡) simultaneous addition, (☆) secondary addition at 60%, (⬠) secondary addition at 70% and (+) secondary addition at 80%. Single catalyst data for (△) Na_2CO_3, (◇) Cs_2CO_3, (□) $CaCO_3$ and (○) $BaCO_3$ are reproduced for reference (open symbols R/C 100, and closed symbols R/C 200).

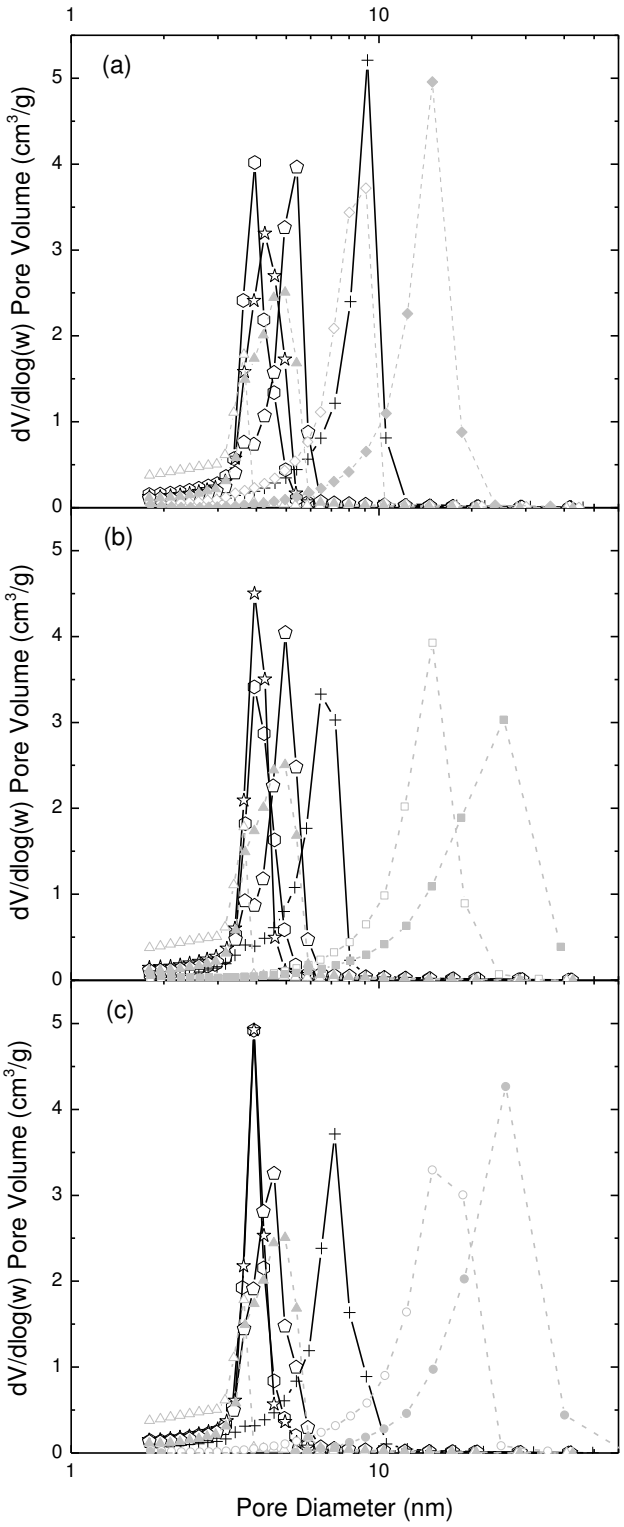

Figure 6. Pore size distributions for (a) Cs_2CO_3/Na_2CO_3, (b) $CaCO_3/Na_2CO_3$ and (c) $BaCO_3/Na_2CO_3$ at (⬡) simultaneous addition, (☆) secondary addition at 60%, (⬠) secondary addition at 70% and (+) secondary addition at 80%. Single catalyst data for (△) Na_2CO_3, (◇) Cs_2CO_3, (□) $CaCO_3$ and (○) $BaCO_3$ are reproduced for reference (open symbols R/C 100, and closed symbols R/C 200).

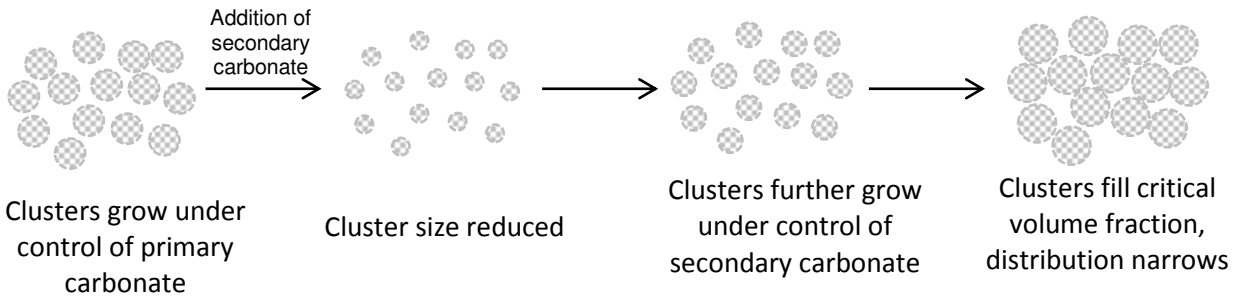

Figure 7. Schematic diagram illustrating the growth of clusters after addition of the secondary metal carbonate. Clusters are depicted as spheres for clarity.

Table 1. Textural properties of single catalyst gels prepared in this study.

R/C	S_{BET} (m^2/g)	V_{TOT} (cm^3/g)	V_{μ} (cm^3/g)	d_p avg. (nm)
		Na_2CO_3[a]		
100	533 ± 5	0.35	0.05	2.9
200	508 ± 4	0.54	0.03	4.2
		Cs_2CO_3[a]		
100	425 ± 3	0.72	0.02	6.9
200	329 ± 3	0.98	0.02	12.6
		$CaCO_3$		
100	307 ± 3	0.88	0.02	12.4
200	301 ± 3	1.14	0.02	17.6
		$BaCO_3$		
100	331 ± 3	1.11	0.01	13.3
200	275 ± 3	1.33	0.02	21.8

[a]Data for Na_2CO_3 and Cs_2CO_3 reproduced from Taylor *et al*.[8]

Table 2. Metal carbonate combinations for mixed catalyst gels prepared in this study.

Primary Metal Carbonate	Secondary Metal Carbonate
Cs	Na
Ca	Na
Ba	Na

Table 3. Textural properties of mixed catalyst gels prepared in this study.

Secondary Addition Point	S_{BET} (m^2/g)	V_{TOT} (cm^3/g)	V_{μ} (cm^3/g)	d_p avg. (nm)
		Cs_2CO_3/Na_2CO_3		
Simultaneous	537 ± 4	0.51	0.04	3.8
60%	520 ± 4	0.53	0.03	4.0
70%	498 ± 4	0.56	0.03	4.6
80%	457 ± 4	0.75	0.03	7.3
		$CaCO_3/Na_2CO_3$		
Simultaneous	535 ± 4	0.56	0.03	4.2
60%	533 ± 4	0.51	0.03	3.8
70%	526 ± 5	0.63	0.04	5.0
80%	490 ± 4	0.64	0.04	5.5
		$BaCO_3/Na_2CO_3$		
Simultaneous	548 ± 5	0.54	0.04	4.0
60%	535 ± 4	0.51	0.04	3.8
70%	528 ± 4	0.55	0.03	4.1
80%	486 ± 4	0.69	0.04	6.1

TOC Graphic

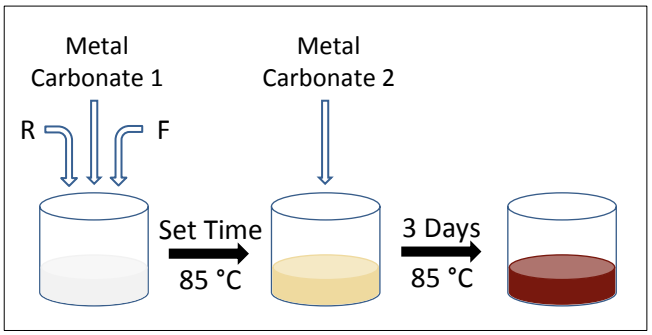
Metal
Carbonate 1
R
F
Set Time
85 °C
Metal
Carbonate 2
3 Days
85 °C